Characteristics of angular precision and dilution of precision for optical wireless positioning

Mark H. Bergen, *Student Member, IEEE,* Ahmed Arafa, *Student Member, IEEE,* Xian Jin, *Student Member, IEEE,* Richard Klukas, *Member, IEEE,* and Jonathan F. Holzman, *Member, IEEE*

***Abstract*—The challenges of optical wireless positioning are addressed in this work, by a thorough investigation of angle of arrival (AOA) positioning characteristics. The overall positioning precision for AOA positioning is studied in terms of two contributing factors—being angular precision and geometric dilution of precision (DOP). Angular precision is characterized for an optical wireless receiver having an especially wide angular field-of-view (FOV). Geometric DOP is characterized for optical beacons deployed in the form of triangle, square, and hexagon cell geometries. The mean and standard deviation of the positioning errors are extracted from the positioning error distributions for each of the three cell geometries. It is found that the overarching goal to establish low and uniform positioning error distributions can be met by implementing an optical wireless receiver with a wide angular FOV and by implementing the optical beacon geometry with a correspondingly small height-to-side-length ratio. The prospects of these findings are discussed for future optical wireless positioning systems.**

***Index Terms*—Angle of arrival, dilution of precision, optical wireless positioning.**

I. Introduction

OPTICAL wireless networks are increasingly attractive implementations for indoor networks. Optical wireless communication (OWC) systems have been shown to support high data rates [1,2], with performance levels that can surpass those of traditional radio-frequency Wi-Fi communication networks [3]. Likewise, Optical wireless location (OWL) systems have been shown to support accurate indoor positioning [4], with performance levels that can surpass those of radio-frequency Wi-Fi positioning networks [3]. OWL systems, in particular, are now emerging as tandem positioning-communication systems or as dedicated positioning systems [5], through rivaling implementations.

The standard OWL implementation is based upon received signal strength (RSS) positioning [6]. An RSS positioning system employs overhead optical beacons, typically comprised of light emitting diode (LED) transmitters, along with a mobile optical wireless receiver, typically consisting of a single photodetector. The optical wireless receiver detects incident optical powers from the distributed optical beacons, and uses a prescribed algorithm to weight these incident optical powers and estimate its position. The fundamental challenge associated with this RSS positioning comes about from its computation of position estimates directly from the incident optical powers. It has been found by ourselves [5] and others [7] that such positioning, being based on scalar measurements, i.e., incident optical powers, is susceptible to variations in the optical beacon power levels and radiation patterns. Power imbalances between optical beacons can result in the inaccurate weighting of incident optical powers which subsequently leads to increased positioning errors [8].

Given the fundamental challenge facing RSS positioning, and the complexities of synchronization in alternative high-frequency/broadband positioning systems, such as those employing time of arrival [9, 10,11] and time difference of arrival [12,13], there has emerged interest in OWL implementations based upon angle of arrival (AOA) positioning [4]. AOA positioning uses overhead optical beacons, typically comprised of LED transmitters, along with a mobile optical wireless receiver that is capable of measuring the angle of arrival of incident beams arriving from the distributed optical beacons. The optical wireless receiver uses multiple photodetectors, with differing orientations [14] or imaging lenses [15], to measure an AOA vector toward each observable optical beacon—defined in terms of its azimuthal angle, ϕ, and polar angle, θ. The AOA vectors and known coordinates of the optical beacons are used, via triangulation, to estimate the optical wireless receiver position as the intersection point of the AOA vectors. As AOA positioning is fundamentally based upon vectors, the position estimates are independent of the optical beacon power levels and radiation patterns (for reception above a minimum intensity threshold [5]). This approach allows AOA positioning to be insensitive to power imbalances across optical beacon geometries.

In this work, the key developmental challenges of AOA-based OWL systems are addressed. The angular precision of the optical wireless receiver is analyzed first through a quantification of AOA error. The geometric dilution of precision (DOP) is then analyzed for various optical beacon geometries. Geometric DOP is a characteristic of AOA-based positioning systems that, to the authors' best knowledge, has

Manuscript received ##########; revised ##########; accepted ##########. Date of publication ##########; date of current version ##########. This work was supported in part by the Natural Science and Engineering Research Council of Canada (NSERC), the Canadian Foundation for Innovation (CFI), and Western Economic Diversification Canada (WD).

The authors are with the Faculty of Applied Science, University of British Columbia, Kelowna, BC V1V 1V7, Canada (e-mail: mark.bergen@alumni.ubc.ca; ahmadarafa@gmail.com; xian.jin@ubc.ca; richard.klukas@ubc.ca; jonathan.holzman@ubc.ca).

remained uninvestigated for indoor AOA-based positioning systems. It is found that an optical wireless receiver with a small AOA error across a wide angular field-of-view (FOV) can be deployed with a broadly-distributed optical beacon geometry to yield low and uniform distributions for geometric DOP and three-dimensional (3-D) positioning errors.

The work is organized as follows. Section II characterizes positioning precision, with subsections dedicated to the two contributing factors, being angular precision and geometric DOP. Section III shows results for AOA positioning in OWL systems having various optical beacon geometries. Section IV draws some concluding remarks.

II. POSITIONING PRECISION

An AOA-based positioning system has a fixed optical beacon geometry and a mobile optical wireless receiver. The optical wireless receiver measures an AOA for each observed optical beacon. The AOA is defined by both an azimuthal angle, ϕ, and a polar angle, θ, in the (x',y',z') coordinates of its body frame. Each AOA defines a line of position (LOP), as a vector, directed from the optical beacon to the optical wireless receiver. The LOPs are used to triangulate the optical wireless receiver's position, as the intersection of all the LOPs, in the (x,y,z) coordinates of the global frame. If the body frame orientation is known, with respect to the global frame, triangulation is applied using two or more optical beacons. If the body frame orientation is unknown, with respect to the global frame, triangulation is applied using three or more optical beacons. Note that positioning with greater numbers of optical beacons yields improved positioning performance.

Precision for AOA positioning is dictated by the angular precision of the optical wireless receiver and the geometric DOP of the optical beacon geometry. In Section IIA, angular precision is quantified by the AOA error, σ_a, which is shown to be constant over a range of azimuthal and polar angles. In Section IIB, geometric DOP(x,y,z) is analyzed according to its definition—as the ratio of the positioning error distribution, $\sigma_p(x,y,z)$, in the (x,y,z) coordinates of the global frame, to the constant AOA error, σ_a [16,17]. Thus, precision for AOA positioning is quantified by the positioning error distribution,

$$\sigma_p(x,y,z) = \sigma_a \cdot \mathrm{DOP}(x,y,z)\,, \qquad (1)$$

where the position of the optical wireless receiver is defined in the global frame by the coordinates (x,y,z).

The multiplicative factors in (1) can be visualized with Figs. 1(a) and (b). The finite AOA error, σ_a, manifests itself as an LOP cone, rather than an ideal LOP line/vector, emanating from each optical beacon. The intersecting volume of the LOP cones defines the optical wireless receiver's position estimate (as the centre of the volume) and positioning error (as the statistical side-length of the volume). With this visualization, the optical wireless receiver's positioning error is a function of its position, with respect to the optical beacons. For example, in Fig. 1(a), the optical wireless receiver's position is such that it observes optical beacons with a narrow separation. This has relatively parallel LOPs, which yield a large intersecting volume and large positioning error. In contrast, the optical wireless receiver's position in Fig. 1(b) is such that it observes optical beacons with a wide separation. This has relatively orthogonal LOPs, which yield a small intersecting volume and small positioning error. In general, the geometry-dependent weighting factor that transforms the finite AOA error, σ_a, to the final positioning error distribution, $\sigma_p(x,y,z)$, is defined as the geometric DOP distribution, DOP(x,y,z) [16,17].

Given the above factors for positioning errors, it is beneficial to realize AOA positioning with two characteristics: i. the optical wireless receiver should maintain a small AOA error over a wide angular FOV; ii. the optical beacon geometry should exhibit a low and uniform geometric DOP distribution. These characteristics are addressed in the following subsections. Subsection IIA characterizes the angular precision of the optical wireless receiver, quantified by the AOA error, and subsection IIB characterizes the geometric DOP distribution of the optical beacon geometry.

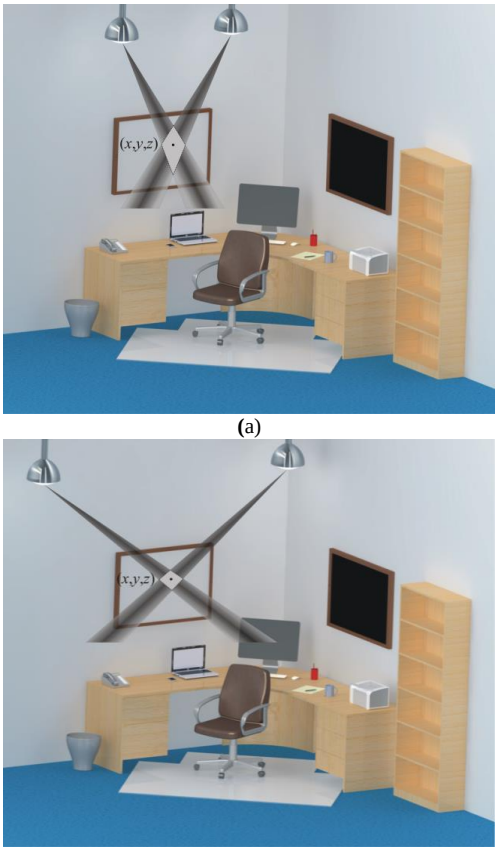

Fig. 1. Schematics are shown for AOA positioning via (a) triangulation using optical beacons at a narrow separation and (b) triangulation using optical beacons at a wide separation. The system is subject to a finite AOA error, which is illustrated as LOP cones in the figures. The intersecting volume of the LOP cones defines a position estimate at (x,y,z) (as the centre of the volume) and a positioning error (as the statistical side-length of the volume).

A. Characterization of angular precision

In this study, the optical wireless receiver is operated over azimuthal and polar angles with negligible systematic errors, i.e., negligible distortion from imaging aberrations, such as coma or astigmatism, making angular precision and accuracy equivalent. Angular precision is quantified here as the AOA

error, σ_a, in (1), and it is the statistical difference between measured and true values for the azimuthal and polar angles.

The AOA error should be as low as possible over as wide of an angular FOV as possible. Our prior work has shown that this need can be met with an optical wireless receiver using a wide-angular-FOV microlens formed by an electro-dispensing process [15]. In this process, a UV-curable polymer microdroplet is dispensed in a filler solution, through a metal needle tip, onto a glass plate, and the voltage on the metal needle tip is varied to tune the microdroplet shape via electrowetting [18]. When the desired shape is achieved, the microdroplet is solidified into a microlens by UV curing. Details of the process are shown elsewhere [18]. For this study, electro-dispensing is used to form a high-contact-angle microlens with a wide angular FOV. A scanning electron microscope (SEM) image of the microlens is shown in Fig. 2(a). The microlens and its glass plate are positioned above an image sensor, with the microlens facing the image sensor. The distance between the microlens and image sensor is adjusted to have collimated light (from a distant source) focus on the plane of the image sensor. The focal spot diameter on the image sensor is approximately 30 µm. This focal spot diameter is deemed to be acceptable for the 6×6 µm^2 CMOS pixels of the image sensor—as smaller focal spot diameters cause pixelation and increase quantization errors in images. An SEM image of the CMOS pixels is shown in Fig. 2(b).

To quantify the AOA error of the optical wireless receiver, the receiver is positioned in a testbed having optical beacons distributed over a range of azimuthal, ϕ, and polar, θ, angles. The optical wireless receiver acquires images of the optical beacons, with each optical beacon forming a focal spot on the image sensor. The precise location of each circular focal spot is recorded, as defined by the geometric mean (i.e., centre) of the intensity profile, on Cartesian coordinates (x_{IS},y_{IS}) that have axes aligned to the centre of the microlens. The optical wireless receiver yields an estimated azimuthal angle, ϕ_{IS} = arctan(y_{IS}/x_{IS}) – 180°, and estimated polar angle, $\theta_{IS} \approx k(x_{IS}^2 + y_{IS}^2)^{1/2}$, where k is a proportionality constant. These angles are estimates of the true azimuthal angle,

$$\phi \approx \phi_{IS} = \arctan(y_{IS}/x_{IS}) - 180°, \quad (2)$$

and the true polar angle,

$$\theta \approx \theta_{IS} \approx k(x_{IS}^2 + y_{IS}^2)^{1/2}. \quad (3)$$

The AOA angle characterization is shown in Fig. 3. In Fig. 3(a), the estimated azimuthal angle, ϕ_{IS}, and azimuthal angle error, $\Delta\phi = \phi_{IS} - \phi$, are seen on respective left and right axes versus the true azimuthal angle, ϕ. In Fig. 3(b), the estimated polar angle θ_{IS}, and polar angle error, $\Delta\theta = \theta_{IS} - \theta$, are seen on respective left and right axes versus the true polar angle, θ.

In this study, deviations from linearity, seen by $\phi \approx \phi_{IS}$ and $\theta \approx \theta_{IS}$, and random measurement errors, seen by $\Delta\phi$ and $\Delta\theta$, are tolerable within an AOA error (standard deviation) of $\sigma_a \approx 1°$. The estimated azimuthal angle on the left axis of Fig. 3(a) shows the desired linear relationship, i.e., $\phi_{IS} \approx \phi$, for all ϕ, with $\theta > 3°$, and the azimuthal angle error on the right axis has a standard deviation within the AOA error of $\sigma_a \approx 1°$. For $\theta < 3°$, the optical beacon is nearly overhead, and it is difficult to define ϕ from the focal spot on the image sensor due to pixelation. The estimated polar angle on the left axis of Fig. 3(b) shows the desired linear relationship, i.e., $\theta_{IS} \approx \theta$, for all ϕ, with $\theta < 60°$, and the polar angle error on the right axis has a standard deviation within the AOA error of $\sigma_a \approx 1°$. For $\theta > 60°$, the optical beacon is imaged at an oblique angle and comatic aberration [15] degrades the linearity between θ and θ_{IS}. While it is not seen here, asymmetry in the microlens can introduce astigmatic aberration to degrade the linearity between ϕ and ϕ_{IS}. Overall, effective imaging is seen for $0° \le \phi \le 360°$ and $3° \le \theta \le 60°$ (for an angular FOV of roughly 120°).

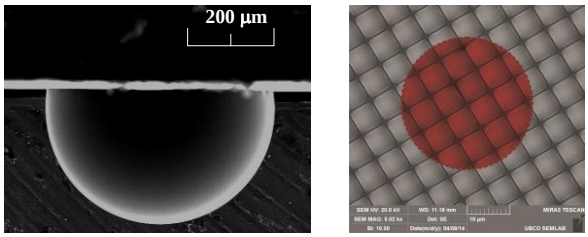

(a) (b)

Fig. 2. SEM images are shown of the (a) microlens that is positioned above the image sensor and (b) CMOS pixels arrayed across the image sensor. The microlens in (a) has a diameter of 500 µm. A visual depiction of the approximate focal spot size is represented in (b) by the dashed/shaded circle.

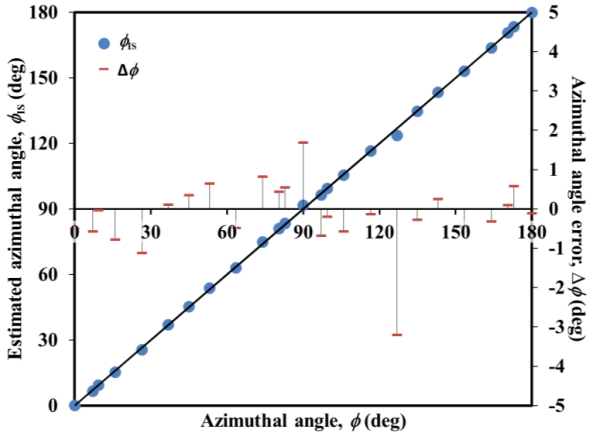

(a)

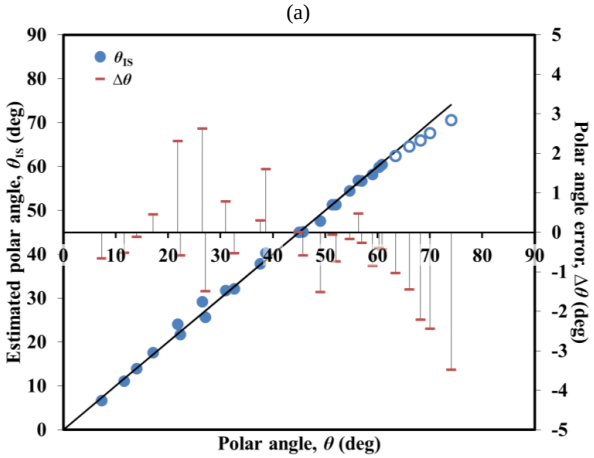

(b)

Fig. 3. Characterizations are shown of the (a) estimated azimuthal angle, ϕ_{IS}, and azimuthal angle error, $\Delta\phi = \phi_{IS} - \phi$, on the left and right axes, respectively, versus the true azimuthal angle, ϕ, and (b) estimated polar angle, θ_{IS}, and polar angle error, $\Delta\theta = \theta_{IS} - \theta$, on the left and right axes, respectively, versus the true

polar angle, θ. Estimated azimuthal and polar angles are depicted by solid and hollow circles inside and outside the angular FOV, respectively. Best-fit lines are applied to angles inside the angular FOV.

B. Characterization of geometric dilution of precision (DOP)

The geometric DOP distribution in this subsection is a geometry-dependent weighting factor that transforms the finite AOA error, σ_a, to the overall positioning error distribution, $\sigma_p(x,y,z)$. Although equivalent in definition to position DOP, which is most often discussed in trilateration systems [16], the term geometric DOP is used here due to the absence of time-based measurements. The geometric DOP distribution is

$$\mathrm{DOP}(x,y,z) = \sqrt{\mathrm{tr}[(H^{\mathrm{T}}H)^{-1}]} = \frac{\sigma_{\mathrm{p}}(x,y,z)}{\sigma_{\mathrm{a}}}, \qquad (4)$$

where tr[·] is the trace operator, $[\cdot]^{\mathrm{T}}$ is the transpose operator, H is the geometric design matrix, and $\sigma_p(x,y,z)$ is the positioning error distribution. For 3-D positioning, least-squares is used to estimate the (x,y,z) position by minimizing the measurement residuals (difference between the observed measurements and the measurements adjusted to yield a unique solution), this yields the positioning error distribution, $\sigma_p(x,y,z)$, seen in (2). The primary assumption here is that the covariance of the measurements in ϕ and θ are equal.

It is seen from (4) that DOP is defined by the geometric design matrix, H, which is formulated according to the global frame coordinates in Fig. 1(a). The optical wireless receiver is positioned at an arbitrary position, (x,y,z), and there exist optical beacons at global coordinates defined by (x_i,y_i,z_i), with optical beacons indexed according to $i = 1, 2, ..., n$. The azimuthal angle, ϕ_i, and polar angle, θ_i, are measured as the AOA toward the i^{th} optical beacon. These angles are related to the optical wireless receiver position at (x,y,z) by

$$\phi_i = \arctan\left(\frac{y-y_i}{x-x_i}\right), \qquad (5)$$

and

$$\theta_i = \arctan\left(\frac{r_i}{|z-z_i|}\right), \qquad (6)$$

where

$$r_i = \sqrt{(x-x_i)^2+(y-y_i)^2}\,. \qquad (7)$$

In addition, the distance from the optical wireless receiver at (x,y,z) to the optical beacon at (x_i,y_i,z_i) is given by

$$R_i = \sqrt{(x-x_i)^2+(y-y_i)^2+(z-z_i)^2}\,. \qquad (8)$$

The geometric design matrix, H, is created from a linearization of the system equations (5) through (8), by forming partial derivatives of ϕ_i and θ_i with respect to x, y, and z. The partial derivatives of ϕ_i in (5) define the azimuthal geometric design matrix, H_ϕ, according to

$$\begin{bmatrix} \partial\phi_1 \\ \vdots \\ \partial\phi_i \\ \vdots \\ \partial\phi_n \end{bmatrix} = [H_\phi]\begin{bmatrix} \partial x \\ \partial y \\ \partial z \end{bmatrix} = \begin{bmatrix} \frac{\partial\phi_1}{\partial x} & \frac{\partial\phi_1}{\partial y} & \frac{\partial\phi_1}{\partial z} \\ \vdots & \vdots & \vdots \\ \frac{\partial\phi_i}{\partial x} & \frac{\partial\phi_i}{\partial y} & \frac{\partial\phi_i}{\partial z} \\ \vdots & \vdots & \vdots \\ \frac{\partial\phi_n}{\partial x} & \frac{\partial\phi_n}{\partial y} & \frac{\partial\phi_n}{\partial z} \end{bmatrix}\begin{bmatrix} \partial x \\ \partial y \\ \partial z \end{bmatrix}. \qquad (9)$$

The partial derivatives of θ_i in (6) define the polar geometric design matrix, H_θ, according to

$$\begin{bmatrix} \partial\theta_1 \\ \vdots \\ \partial\theta_i \\ \vdots \\ \partial\theta_n \end{bmatrix} = [H_\theta]\begin{bmatrix} \partial x \\ \partial y \\ \partial z \end{bmatrix} = \begin{bmatrix} \frac{\partial\theta_1}{\partial x} & \frac{\partial\theta_1}{\partial y} & \frac{\partial\theta_1}{\partial z} \\ \vdots & \vdots & \vdots \\ \frac{\partial\theta_i}{\partial x} & \frac{\partial\theta_i}{\partial y} & \frac{\partial\theta_i}{\partial z} \\ \vdots & \vdots & \vdots \\ \frac{\partial\theta_n}{\partial x} & \frac{\partial\theta_n}{\partial y} & \frac{\partial\theta_n}{\partial z} \end{bmatrix}\begin{bmatrix} \partial x \\ \partial y \\ \partial z \end{bmatrix}. \qquad (10)$$

The geometric design matrix, H, is then defined as augmented azimuthal and polar geometry matrices, according to

$$\begin{bmatrix} \partial\phi_1 \\ \vdots \\ \partial\phi_i \\ \vdots \\ \frac{\partial\phi_n}{\partial\theta_1} \\ \vdots \\ \partial\theta_i \\ \vdots \\ \partial\theta_n \end{bmatrix} = \begin{bmatrix} H_\phi \\ H_\theta \end{bmatrix}\begin{bmatrix} \partial x \\ \partial y \\ \partial z \end{bmatrix} = [H]\begin{bmatrix} \partial x \\ \partial y \\ \partial z \end{bmatrix}, \qquad (11)$$

$$[H] = \begin{bmatrix} \frac{(y_1-y)}{r_1^2} & \frac{(x-x_1)}{r_1^2} & 0 \\ \vdots & \vdots & \vdots \\ \frac{(y_i-y)}{r_i^2} & \frac{(x-x_i)}{r_i^2} & 0 \\ \vdots & \vdots & \vdots \\ \frac{(y_n-y)}{r_n^2} & \frac{(x-x_n)}{r_n^2} & 0 \\ \hline \frac{|z_1-z|(x_1-x)}{r_1R_1^2} & \frac{|z_1-z|(y_1-y)}{r_1R_1^2} & \frac{r_1}{R_1^2} \\ \vdots & \vdots & \vdots \\ \frac{|z_i-z|(x_i-x)}{r_iR_i^2} & \frac{|z_i-z|(y_i-y)}{r_iR_i^2} & \frac{r_i}{R_i^2} \\ \vdots & \vdots & \vdots \\ \frac{|z_n-z|(x_n-x)}{r_nR_n^2} & \frac{|z_n-z|(y_n-y)}{r_nR_n^2} & \frac{r_n}{R_n^2} \end{bmatrix}. \qquad (12)$$

The geometric DOP distribution is then calculated using H within (4). Note that positioning with n optical beacons yields $2n$ rows in the H matrix and an increasingly overdetermined H matrix yields lower $\mathrm{DOP}(x,y,z)$ and $\sigma_p(x,y,z)$ values—as

expected for the least squares algorithm with increasing redundancy in the measurement space.

III. Positioning Results

The characterizations of angular precision and geometric DOP in the prior section quantify the positioning errors for distributions of optical beacons. The optical beacons can be arranged in a single cell [5] or in a periodic array of such cells [13]. In this study, the individual cells are analyzed with optical beacons distributed in (equilateral) triangle, square, and hexagon geometries, as it is only these polygonal geometries that can form regular tessellations, i.e., periodic arrays [13]. The results of this study can be applied to the case of periodic arrays of cells, if desired, by considering that the positioning error distribution of a periodic array of cells can only improve upon that of the single cell.

The cells that are analyzed have their optical beacons arranged in the triangle, square, and hexagon geometries shown in Figs. 4(a), (b), and (c), respectively. For a fair comparison, the area density of the optical beacons, being equivalent to the optical power per unit area, is made equal for the three cell geometries. Thus, the triangle, square, and hexagon cell geometries distribute their 1/2, 1, and 2 optical beacons, indicated by the sums of the areas shaded in blue in Fig. 4, over areas of $\frac{1}{2}\cdot a^2$, $1\cdot a^2$ and $2\cdot a^2$, respectively, where a is the side-length of the square cell geometry.

The positioning error distribution, $\sigma_p(x,y,z=0)$, and geometric DOP distribution, DOP$(x,y,z=0)$, are shown in Figs. 5(a), (b), and (c), for the respective triangle, square, and hexagon cell geometries, given an AOA error of $\sigma_a = 1°$ and $a = 100$ cm. The origin of the global frame coordinate system, $(x=0,y=0,z=0)$, is at the centre of each cell geometry, with the optical beacons at a height $z = h = 100$ cm, and the optical wireless receiver is rastered across the $z = 0$ plane to form the positioning error distributions according to (4). A comparison is carried out on the three cell geometries to identify a positioning error distribution with low magnitudes and good uniformity. For the triangle cell geometry results in Fig. 5(a), the red/yellow colouring and deep undulations of the positioning error distribution suggest that this geometry results in positioning errors with high magnitudes and poor uniformity. This observation is corroborated by the large mean, i.e., expectation value, $E[\sigma_P(x,y,z=0)] = 2.65$ cm, and large standard deviation, $STD[\sigma_p(x,y,z=0)] = 0.095$ cm, for the positioning error distribution. For the square cell geometry results in Fig. 5(b), the green/blue colouring and moderate undulations of the positioning error distribution suggest that this geometry results in positioning errors with average magnitudes and average uniformity. This observation is corroborated by the moderate mean, i.e., expectation value, $E[\sigma_P(x,y,z=0)] = 2.26$ cm, and moderate standard deviation, $STD[\sigma_p(x,y,z=0)] = 0.066$ cm, across the positioning error distribution. For the hexagon cell geometry results in Fig. 5(c), the dark blue colouring and shallow undulations of the positioning error distribution suggest that this geometry forms positioning errors with low magnitudes and good uniformity. This observation is corroborated by the small mean, i.e., expectation value, $E[\sigma_P(x,y,z=0)] = 1.87$ cm, and small deviation, $STD[\sigma_p(x,y,z=0)] = 0.053$ cm, across the positioning error distribution.

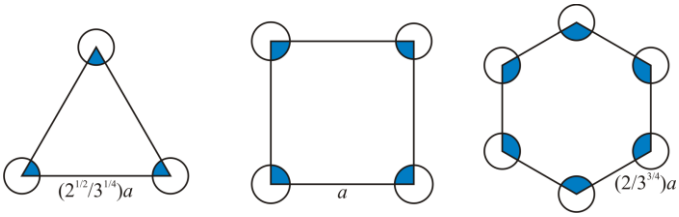

Fig. 4. Optical beacons are shown for the (a) triangle cell geometry, with a side-length of $2^{1/2}/3^{1/4}a$, (b) square cell geometry, with a side-length of a, and (c) hexagon cell geometry, with a side-length of $2/3^{3/4}a$. Optical beacons are shown as circles, with the fraction of each optical beacon being applicable to the given cell geometry shaded in blue. The three cell geometries have an equal area density, corresponding to one optical beacon per area of a^2.

The mean and standard deviation of the positioning errors for the three cell geometries are summarized in Table I, for the prior configuration with $h = a = 100$ cm. From the trends seen here, the hexagon cell geometry is found to yield the most favourable positioning error distribution, because of its small mean and small standard deviation. The benefits of the hexagon cell geometry come about from the requirement for an equal area density of optical beacons—which favours the close-pack nature of the hexagon cell geometry. Having an equal number of optical beacons per unit area forces the optical beacons within the close-packed geometry to be spread apart, compared to the spacings of the other two geometries, and this spreading benefits AOA positioning. For the hexagon cell geometry the optical wireless receiver images the spread optical beacons with LOPs that are more orthogonal, compared to those of the other two geometries, and this yields reduced values for the geometric DOP and positioning error.

In general, the characteristics of the positioning error distributions for the three cell geometries will depend upon the ratio of the optical beacon geometry's height, h, to side-length, a, and the h/a values that can be implemented will depend upon the angular FOV of the specific optical wireless receiver used. With this in mind, the mean and standard deviation of the positioning error distribution, $\sigma_p(x,y,z=0)$, and geometric DOP distribution, DOP$(x,y,z=0)$, are extracted for the three cell geometries and displayed in Fig. 6, as a function of the h/a ratio. In Fig. 6(a), the mean of the positioning error distribution, $E[\sigma_P(x,y,z=0)]$, and geometric DOP distribution, $E[DOP(x,y,z=0)]$, are shown. It is seen that there is a general trend for the mean values to increase with the h/a ratio. (A slight decrease in the mean values is seen for $h/a < 0.25$, although such a regime is deemed to be impractical and not of interest to this investigation.) The increase in mean values is because positioning error increases along with the height of the optical beacons, as expected due to the increasing intersecting volume of the LOP cones in Fig. 1 resulting from an increasing height. In Fig. 6(b), the standard deviation of the positioning error distribution, $STD[\sigma_p(x,y,z=0)]$, and geometric DOP distribution, $STD[DOP(x,y,z=0)]$, are shown. It is seen that

there is an optimal window over which small and uniform positioning error standard deviations are achieved for the triangle, square, and hexagon cell geometries. The optimal window is shown in Figs. 6(a) and (b), as h/a ratios ranging from approximately 0.5 to 2.0.

The overarching goal to establish a low and uniform positioning error distribution leads to design constraints for the optical beacon geometry and the optical wireless receiver. According to Fig. 6(a), the optical beacon geometry should be implemented with an h/a ratio that is as small as possible, to form a low positioning error distribution, and it should be implemented within the optimal window for the h/a ratio in Fig. 6(b), to form a uniform positioning error distribution. With the above design constraints in mind, the optical wireless receiver should be implemented with as wide an angular FOV as possible. This is because the angular FOV of the optical wireless receiver defines the minimum allowable h/a ratio below which the optical wireless receiver is not able to image all optical beacons in the geometry. The minimum allowable h/a ratio is defined here, conservatively, by the condition for imaging at the extremes of each cell geometry—with the optical wireless receiver imaging an optical beacon in the corner while it is positioned in the opposite corner. It can be shown that the minimum allowable h/a ratio is given by 1/tan(FOV/2), $2^{½}$/tan(FOV/2), and 2/tan(FOV/2), for the triangle, square, and hexagon cell geometries, respectively.

Given the above design constraints, Figs. 6(a) and (b) identify the minimum h/a ratios for the 120° angular FOV of the developed optical wireless receiver. The minimum h/a ratios are 0.58, 0.82, and 1.15 for the triangle, square, and hexagon cell geometries, respectively. The three optical beacon geometries, with these minimum h/a ratios, yield a similar mean for the positioning error distribution, $E[\sigma_P(x,y,z=0)] \approx 1.8$ cm, and a similar standard deviation for the positioning error distribution, $STD[\sigma_P(x,y,z=0)] \approx 0.05$ cm. The main consideration for selecting one of the three geometries would be that they achieve these same strong performance levels with optical beacons spread over differing areas. The other consideration worth noting is that these strong performance levels are a direct result of the wide angular FOV of the optical wireless receiver. If the angular FOV is reduced to 60°, the standard angular FOV for an optical wireless receiver, the minimum h/a ratios increase to 1.73, 2.45, and 3.46 for the triangle, square, and hexagon cell geometries, respectively. In such cases, it becomes difficult to meet the goal of simultaneously establishing a low and uniform positioning error distribution.

In general, it can be concluded that OWL systems should be designed with simultaneous considerations for the optical wireless receiver and the optical beacon geometry. The optical wireless receiver should be implemented with as wide of an angular FOV as possible, and the optical beacon geometry should be implemented with the minimum h/a ratio for the angular FOV of the given optical wireless receiver. The positioning performance of the resulting OWL systems can benefit greatly from these careful considerations.

TABLE I
MEAN AND STANDARD DEVIATION OF THE POSITIONING ERROR DISTRIBUTION FOR THE THREE CELL GEOMETRIES

Cell geometry	Positioning error distribution ($h = a = 100$ cm)	
	Mean, $E[\sigma_P(x,y,z=0)]$ [cm]	Standard deviation, $STD[\sigma_P(x,y,z=0)]$ [cm]
Triangle	2.65	0.095 (3.6% of the mean)
Square	2.26	0.066 (2.9% of the mean)
Hexagon	1.87	0.053 (2.8% of the mean)

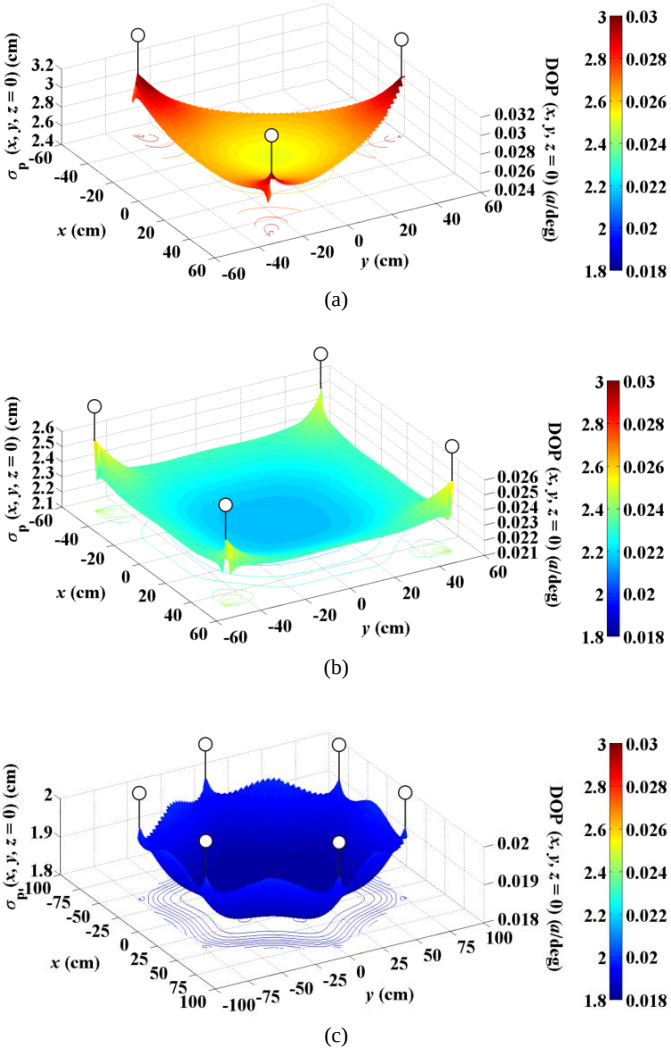

Fig. 5. The positioning error distribution, $\sigma_P(x,y,z=0)$, and geometric DOP distribution, $DOP(x,y,z=0)$, are shown for an optical wireless receiver rastered across the $z = 0$ plane, with optical beacons arranged in the (a) triangle cell geometry, (b) square cell geometry, and (c) hexagon cell geometry. The global frame coordinate axes, i.e., (x=0,y=0,z=0), are defined in the centre of the cell geometries. The optical beacons, represented by hollow circles, are configured with a =100 cm, at a height $z = h$ = 100 cm above the plane of positioning.

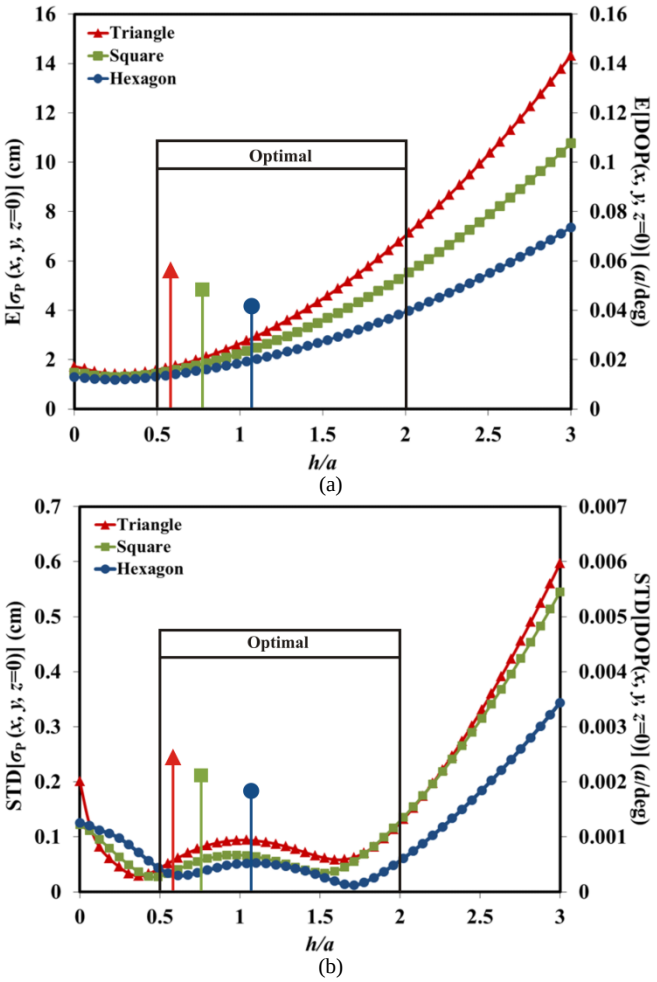

Fig. 6. The (a) mean of the positioning error distribution, E[$\sigma_p(x,y,z=0)$], and geometric DOP distribution, E[DOP(x,y,z=0)], and (b) standard deviation of the positioning error distribution, STD[$\sigma_p(x,y,z=0)$], and geometric DOP distribution, STD[DOP(x,y,z=0)], for the triangle (red), square (green), and hexagonal (blue) cell geometries, shown as a function of the normalized height-to-side-length ratio, h/a, between the optical beacons and optical wireless receiver. The optimal window for the h/a ratio is shown to be between 0.5 and 2.0. Vertical markers are shown for the minimum h/a ratios for the triangle (red), square (green), and hexagonal (blue) cell geometries.

IV. Conclusions

This work presents design considerations for optical wireless systems carrying out AOA-based positioning. Angular precision (pertaining to the optical wireless receiver) and geometric DOP (pertaining to the overall optical wireless system) were studied. An optical wireless receiver with a wide angular FOV was applied, and its angular precision was characterized. Various optical beacon cell geometries were formed, being triangular, square, and hexagonal, and their geometric DOP distributions were characterized. For each geometry, the mean and standard deviation of the positioning errors were extracted from the positioning error distribution. It was found that low and uniform positioning error distributions can be achieved with an optical wireless receiver having a wide angular FOV and an optical beacon geometry with a small height-to-side-length ratio. The presented observations and conclusions can support the design and implementation of future optical wireless systems.

Acknowledgment

The authors would also like to thank Blago Hristovski.

References

[1] K. Wang, A. Nirmalathas, C. Lim, and E. Skafidas, "High-speed optical wireless communication system for indoor applications," *IEEE Photon. Technol. Lett.*, vol. 23, no. 8, pp. 519–521, Apr. 2011.

[2] K. Wang, A. Nirmalathas, C. Lim, and E. Skafidas, "4 x 12.5 Gb/s WDM optical wireless communication system for indoor applications," *J. Lightw. Technol.*, vol. 29, no. 13, pp. 1988–1996, Jul. 2011.

[3] H. Liu, H. Darabi, P. Banerjee, and J. Liu, "Survey of wireless indoor positioning techniques and systems," *IEEE Trans. Syst., Man., Cybern. C*, vol. 37, no. 6, pp. 1067–1080, Nov. 2007.

[4] A. Arafa, X. Jin, and R. Klukas, "Wireless indoor optical positioning with a differential photosensor," *IEEE Photon. Technol. Lett.*, vol. 24, no. 12, pp. 1027–1029, Jun. 2012.

[5] A. Arafa, S. Dalmiya, R. Klukas, and J. F. Holzman, "Angle-of-arrival reception for optical wireless location technology," *Opt. Express*, vol. 23, no. 6, pp. 7755–7766, Mar. 2015.

[6] P. Bahl and V. N. Padmanabhan, "RADAR: an in-building RF-based user location and tracking system," in *Proc. IEEE INFOCOM*, 2000, vol. 2, pp. 775–784.

[7] X. Zhang, J. Duan, Y. Fu, and A. Shi, "Theoretical accuracy analysis of indoor visible light communication positioning system based on received signal strength indicator," *J. Lightw. Technol.*, vol. 32, no. 21, pp. 4180–4186, Nov. 2014.

[8] Y. Kim, J. Hwang, J. Lee, and M. Yoo, "Position estimation algorithm based on tracking of received light intensity for indoor visible light communication systems," in *Proc. IEEE ICUFN Conf.*, 2011, pp. 131–134.

[9] B. Alavi and K. Pahlavan, "Modeling of the TOA-based distance measurement error using UWB indoor radio measurements," *IEEE Commun. Lett.*, vol. 10, no. 4 , pp. 275–277, Apr. 2006.

[10] G. Ding, Z. Tan, L. Zhang, Z. Zhang, and J. Zhang, "Hybrid TOA/AOA cooperative localization in non-line-of-sight environments," in *Proc. IEEE VTC*, 2012, pp. 1–5.

[11] T. Q. Wang, Y. A. Sekercioglu, A. Neild, and J. Armstrong, "Position accuracy of time-of-arrival based ranging using visible light with application in indoor localization systems," *J. Lightw. Technol.*, vol. 31, no. 20, pp. 3302–3308, Oct. 2013.

[12] S.-Y. Jung, S. Hann, and C.-S. Park, "TDOA-based optical wireless indoor localization using LED ceiling lamps," *IEEE Trans. Consum. Electron.*, vol. 57, no. 4, pp. 1592–1597, Nov. 2011.

[13] A. Taparugssanagorn, S. Siwamogsatham, and C. Pomalaza-Ráez, "A hexagonal coverage LED-ID indoor positioning based on TDOA with extended kalman filter," in *IEEE 37th Annual COMPSAC*, 2013, pp. 742–747.

[14] X. Jin and J. F. Holzman, "Differential retro-detection for remote sensing applications," *IEEE Sensors J.*, vol. 10, no. 12, pp. 1875–1883, Dec. 2010.

[15] X. Jin, D. Guerrero, R. Klukas, and J. F. Holzman, "Microlenses with tuned focal characteristics for optical wireless imaging," *Appl. Phys. Lett.*, vol. 105, no. 3, pp. 031102 (1–5), Jul. 2014.

[16] P. Misra and P. Enge, *Global Positioning System – Signals, Measurements, and Performance*, 2nd ed. Lincoln, MA: Ganga-Jamuna Press, 2011, pp. 200–206.

[17] A. G. Dempster, "Dilution of precision in angle-of-arrival positioning systems," *Electron. Lett.*, vol. 42, no. 5, pp. 291–292, Mar. 2006.

[18] B. Born, E. L. Landry, and J. F. Holzman, "Electrodispensing of microspheroids for lateral refractive and reflective photonic elements," *IEEE Photon. J.*, vol. 2, no. 6, pp. 873–883, Dec. 2010.